

https://doi.org/10.1070/QEL16665

Quantum electrodynamic cascade structure in a standing linearly polarised wave

A.V. Bashinov, P. Kumar, A.V. Kim

Abstract. **We have performed an analysis of plasma structures formed as a result of the quantum electrodynamic (QED) cascade development in the field of a standing linearly polarised plane wave at various field amplitudes. In view of the spatially inhomogeneous cascade dynamics and complicated particle motion, it is proposed to use spatial distributions of plasma density averaged over the half-period of the field, i.e. integral structures. Based on the analysis of of particle trajectories and integral structures with and without allowance for the QED cascade, various plasma structures are revealed and the amplitude thresholds of their occurrence are determined. It is shown that the integral structure maxima may arise not only at the electric field nodes or antinodes, as in a circularly polarised field, but also in the intermediate regions between them.**

Keywords: *radiation friction, quantum electrodynamic cascade, electron–positron plasma.*

1. Introduction

A quantum electrodynamic (QED) cascade [1] is one of the expected processes that can be initiated in experiments on multi-petawatt laser facilities [2–4]. The nature of a QED cascade in superstrong laser fields consists in the emission of gamma photons by oscillating electrons and positrons and in the subsequent decay of emitted photons into electron–positron pairs [5]. Recent studies show that the cascade initiation at optimal focusing requires a total laser power of about 5–8 PW [6–8], the target ionisation [9, 10] and its initial density [11] being of great importance. When the rate of production of new pairs exceeds the rate of their losses (for example, the rate of escape from the region of production), an exponential increase in plasma density is observed.

As long as the density is less than the critical value with allowance for relativistic effects, the cascade develops in a linear regime, and the plasma effect on the field can be neglected. Otherwise, when the density reaches the critical value, a nonlinear regime is realised, in which plasma has a significant effect on the radiation that generates plasma. In particular, the produced plasma causes strong absorption of incident radiation [12–16], which limits the maximum achievable field intensities and may also lead to the development of instabilities and the formation of extreme plasma states [17, 18]. The importance of the linear stage is that it largely determines which self-consistent plasma field structures will be formed at the cascade's nonlinear stage. In addition, at the linear stage, photons with the highest energy are generated [7], the spectrum of which depends on the plasma spatial distribution [19].

Note that plasma structures at the linear stage have been actively studied in the fields of colliding laser beams [20–27]. In particular, in the case of circular polarisation, the analysis of structures was carried out not only numerically, but also analytically [25, 27], which is stipulated by a relatively simple particle motion. In this case, the motion can be decomposed into a rotation in the electric field plane and a drift from the field antinode to the field node. If the cascade develops slowly, the particle drift causes the plasma localisation at the field node. However, with the rapid cascade development, the particle escape from the antinode towards the node can be compensated for, and plasma can be localised both at the antinode and simultaneously at the node and antinode, depending on the field amplitude.

In this paper we consider in more detail the case of linearly polarised radiation, which is of great practical importance. The particle motion in a linearly polarised field is more complicated and, as a consequence, the spatiotemporal structure of the cascade also becomes more complicated. In contrast to the circularly polarised field, not only an unstable equilibrium position at the field antinode and an attractor at the field node exist in the case of linear polarisation (ponderomotive trapping and normal radiative trapping (NRT) [27–30]), but also an attractor near the field antinode is formed, which is caused by radiation losses (anomalous radiative trapping (ART) [29, 30]). In addition, oscillations at the oscillation frequency of the Poynting vector are clearly distinguished in the spatiotemporal structure of the cascade [22]. Particle motion complexity and complex structure of the cascade, on the one hand, complicate theoretical analysis, thus making numerical modelling the main tool of investigation, and on the other hand, lead to a variety of plasma-field structures.

Despite the fact that a number of studies have been dedicated to linear structures in the field of counterpropagating linearly polarised laser pulses [22–24, 26], the dependence of these structures on the laser parameters has not yet been sufficiently studied. This paper answers the question of what plasma-field structures can be formed in the field of a plane linearly polarised standing wave, depending on its amplitude at the linear stage of the cascade. First, we present a detailed analysis of the motion of particles and their distribution without allowance for the QED cascade. We then show how these

A.V. Bashinov, A.V. Kim Institute of Applied Physics, Russian Academy of Sciences, ul. Ul'yanova 46, 603950 Nizhniy Novgorod, Russia, e-mail: abvk@inbox.ru;
P.Kumar Department of Physics, University of Lucknow, Lucknow-226007, India

Received 23 February 2018; revision received 29 June 2018
Kvantovaya Elektronika **48** (9) 833–842 (2018)
Translated by M.A. Monastyrskiy

structures are modified by quantum processes. In addition, the rate of particle escape from the field antinode and the cascade growth rate are considered as functions of the field amplitude, which to a large extent determines the threshold values of the amplitudes at which the plasma structure changes.

We should note that in the case of a plane wave, there is no cascade's amplitude threshold for a contnuous signal, since there are no particle losses. However, at the electric field amplitudes $a \ll 1000$ (in relativistic units), the cascade growth rate $\Gamma_{cs} \ll 1$ normalised to a reciprocal of field period is much less than unity [26], and the cascade does not change the structure of electron–positron plasma caused only by particle motion. The amplitude is $a = eE_0/(m\omega c)$, where m and e are the electron mass and charge, respectively; E_0 is the electric field amplitude; c is the speed of light; and $\omega = 2.36 \times 10^{15}$ s^{-1} is the field frequency (the wavelength $\lambda = 0.8$ μm). For $a < 1$, plasma oscillates around the field node in the regime of ponderomotive trapping. For $1 < a < 600$, particles can be trapped into the node region for a random time interval and then leave this region and move along the Poynting vector [28, 31–33], i.e. relativistic chaos is realised. On average, this leads to maximisation of the particle density near the nodes. It should also be noted that the above regimes do not disappear when the amplitude increases, only their 'basins' change, i.e. the phase space volumes from which the particles can be captured into this or that regime. For example, at relativistic amplitudes, the spatial size of the 'basin' of ponderomotive trapping is limited to the range of $\lambda/(2\pi a)$ values, and the particles are stronger localised in the electric field node vicinity than in the NRT regime [31].

Below we present a detailed analysis of plasma structures in the fields with amplitudes of $500 < a < 10000$, at which all motion regimes can be realised, and when not only the radiation losses are of importance, but also the cascade itself, the growth rate of which, at the field amplitudes considered, varies within the range of $1.7 \times 10^{-2} < \Gamma_{cs} < 12.7$. This range of amplitudes corresponds to a wide range of intensities 5×10^{23} W cm^{-2} $< I < 2 \times 10^{26}$ W cm^{-2}, which are planned to be achieved on the multipetawatt laser facilities being designed, for example, XCELS [4].

2. Particle density distribution in the field of a standing linearly polarised wave without taking the cascade into account

Consider the dynamics of particles in the field of a standing plane linearly polarised wave:

$$\boldsymbol{E} = E_0 \cos(\omega x/c)\cos(\omega t)\boldsymbol{z},$$
$$\boldsymbol{B} = -E_0 \sin(\omega x/c)\sin(\omega t)\boldsymbol{y} \quad (1)$$

($\boldsymbol{E}$, $\boldsymbol{B}$ are the electric and magnetic fields directed along the z and y axes, respectively; t is the time; and the x axis is directed along the Poynting vector) and determine which plasma structures can be formed. Let the particles, initially at rest, be evenly distributed in space. To analyse the emerging plasma structures, we use the PICADOR programme [34] based on the particle-in-cell method. In this program, a module [35] is implemented, which allows the stochastic emission of photons in a semiclassical approximation [36] and the decay of photons into pairs in a laser field [5] to be modelled. Since the wave is plane, it is sufficient to use a one-dimensional space modification of the programme. The size of the simulation box was equal to the wavelength $\lambda = 0.8$ μm, the number of cells was 128, and the time step was $0.005T$, where $T = 2.7$ fs was the wave period. Periodic boundary conditions were set for the particles, which corresponded to the mapping of the x axis onto the segment $-0.5\lambda < x < 0.5\lambda$. Note that in the PICADOR programme the particles are not bound to cells, i.e. the particle coordinates are not conditioned by the discretisation in space and may take arbitrary values. In this regard, as many as 256 points on the considered segment are used to retrieve the particle distributions in order to reveal all their features. This technique is valid at the linear stage of the cascade, when the plasma back reaction can be neglected, and also it saves the computational resources.

To avoid the influence of leading edges of laser pulses, we set a standing wave formed in the entire simulation box and resting electrons (positrons) evenly distributed over the entire computational region at the initial time moment. The phase of the initial wave corresponds to a zero magnetic field; however, as the computer simulation shows, the steady-state plasma structures do not depend on that phase. Since the linear stage of the cascade was considered, the initial particle density was chosen to be sufficiently small ($n_0 = 0.01$ cm^{-3}) to ensure that, as a result of the cascade development, the plasma produced would not change the field that forms the plasma. In the linear regime, the initial density determines the lifetime of this regime rather than affects the shape of plasma structures. The initial number of macroparticles in the simulation was 10^5 cm^{-2} (this physical dimension for the number of particles appears in one-dimensional modelling), i.e., about 800 cm^{-2} macroparticles in the cell, one real particle corresponding to about 10^{11} macroparticles.

In one-dimensional geometry, spatial structures with a period of 0.5λ are formed, which is stipulated by periodic variation in the Poynting vector magnitude in space. These structures also possess a reflective symmetry with respect to the axes passing through the electric field nodes or antinodes; therefore, all information about the structure is contained within the segment $0 < x/\lambda < 0.25$. Another property of such structures is that they are nonstationary in time and oscillate with a doubled field frequency (with a frequency of Poynting vector oscillation). Moreover, the oscillation phase difference for electron density and fields is determined by the radiation losses increasing with the wave amplitude, by analogy with the forced oscillations of a harmonic oscillator with allowance for dissipation [37]. This fact may lead to incorrect conclusions about the plasma dynamics if we only consider plasma structures at a certain phase of the field. Due to all these factors, we analysed the electron density distribution integrated over the half-period of the field. This approach does not allow exact distribution of electrons to be restored at a certain time moment, but makes it possible to determine the qualitative changes in their spatial structure. Relevant changes can be reflected in the integral structure if, firstly, they are noticeable in instantaneous distributions and, secondly, if they remain for a considerable time during the half-period of the field.

In numerical simulation, the electron densities $n_k(x)$ at each kth time step, divided by the total number $N_{\Sigma k}$ of particles at a given time moment in the entire simulation box, were summed up at each point x_i of space, and the result was divided by the total number N_t of time steps within the half-

period of the field and by the maximum value M of the total electron density distribution:

$$n_{\rm st}(x_i) = (N_{\rm t} M)^{-1} \sum_{k=1}^{N_{\rm t}} n_k(x_i) N_{\Sigma k}^{-1}. \qquad (2)$$

The steady-state integral structure and instantaneous distributions at various time moments

$$n_{\rm e}(x) = n_k(x)(N_{\Sigma k} M)^{-1} \qquad (3)$$

corresponding to the case of the most complex spatiotemporal dynamics of electrons are shown in Fig. 1. It is seen that, on the whole, the integral structure reproduces the maxima observed in the dynamics of the electron density. However, the exception is a maximum near $x = 0.21\lambda$, observed for a short time, $14.53 < t/T < 14.56$.

Figure 2 shows the steady-state integral structures for various field amplitudes. The issue of relaxation time for integral structures has not been studied in detail; however, as numerical simulation shows, by the time $t = 15T$, the structures became steady-state for all the field amplitudes under consideration. At amplitudes $a < 600$, the particle motion occurs in the regime of relativistic chaos. Due to the fact that the particles, diffusively propagating along the x axis, fall for random time intervals into the node region, the particle density maximum at $x = 0.25\lambda$ is clearly visible. Examples of particle trajectories in this regime are shown in Figs 3a and 3d. To analyse the particle motion, the motion equations were solved numerically with allowance for radiative losses, which were modelled in the quasi-classical approximation (stochastic radiation) [31, 36] or described using the Landau–Lifshitz force with allowance for quantum corrections [20, 27].

At larger amplitudes ($a > 600$), the radiation effects start to play an important role in the particle dynamics and the NRT regime arises, in which the particles are attracted to a field node. Note that in the case of circular polarisation, the corresponding threshold amplitude is equal to 70 [27]. In the case of linear polarisation, the oscillations of the Poynting vector and, as a consequence, of the longitudinal driving

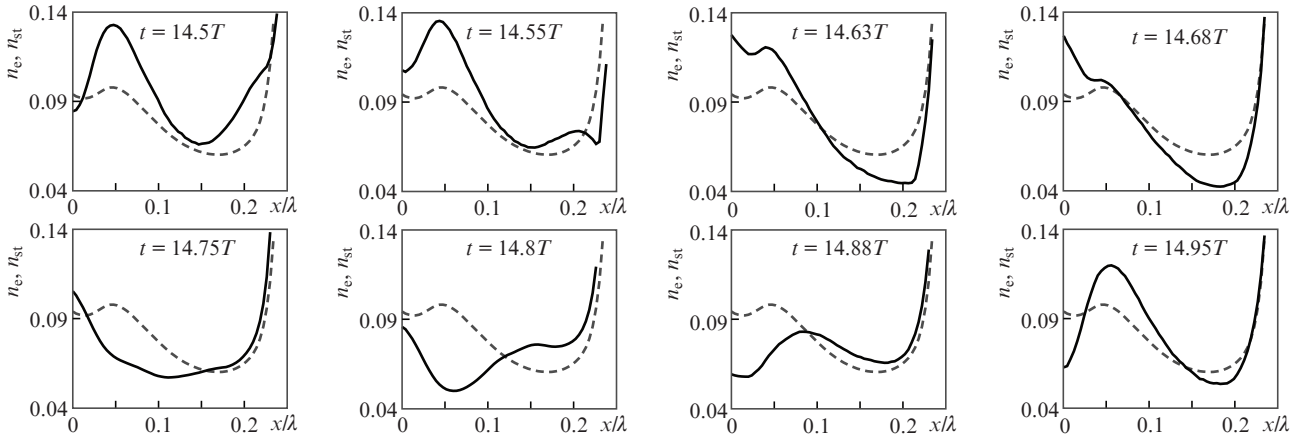

Figure 1. Instantaneous ($n_{\rm e}$, solid curves) and integral ($n_{\rm st}$, dashed curves) electron density distributions in the field of a plane standing linearly polarised wave at an amplitude of $a = 3500$, obtained during the half-period of the field.

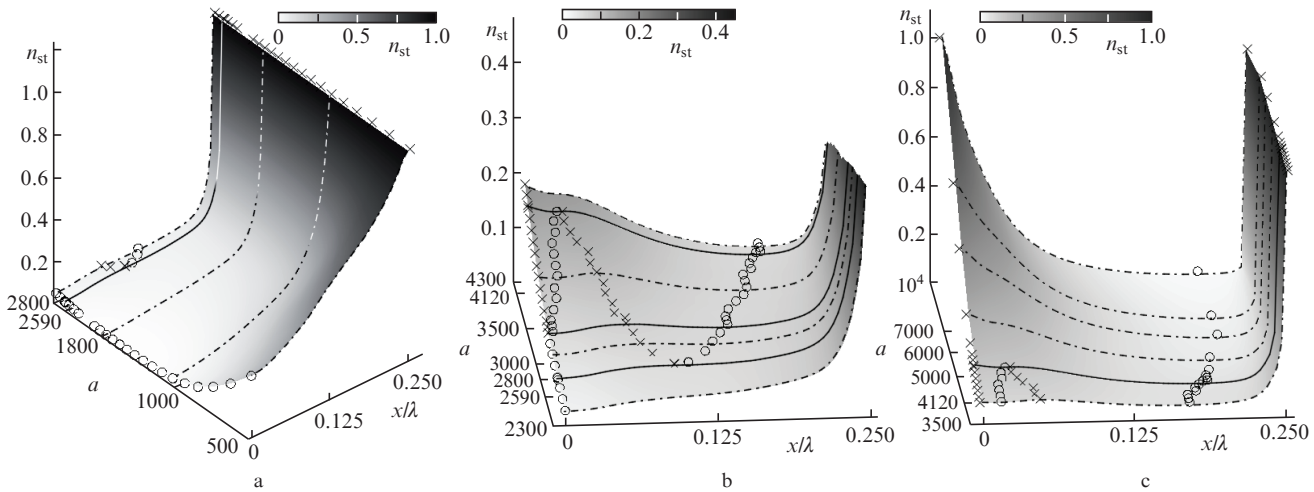

Figure 2. Steady-state integral structures for various field amplitude ranges: (a) $a \in [500, 2800]$, (b) $a \in [2300, 4300]$, and (c) $a \in [3500, 10^4]$. Solid curves are the integral structures at threshold field amplitudes, dashed curves are the examples of integral structures at various regimes. For each curve (solid and dashed), the corresponding field amplitude is indicated. Points indicate local minima (○) and maxima (×). For clarity, the integral structures in Fig. 2b are cut off at the level $n_{\rm st} = 0.45$, as a result of which the maxima at point $x = 0.25\lambda$ are not visible.

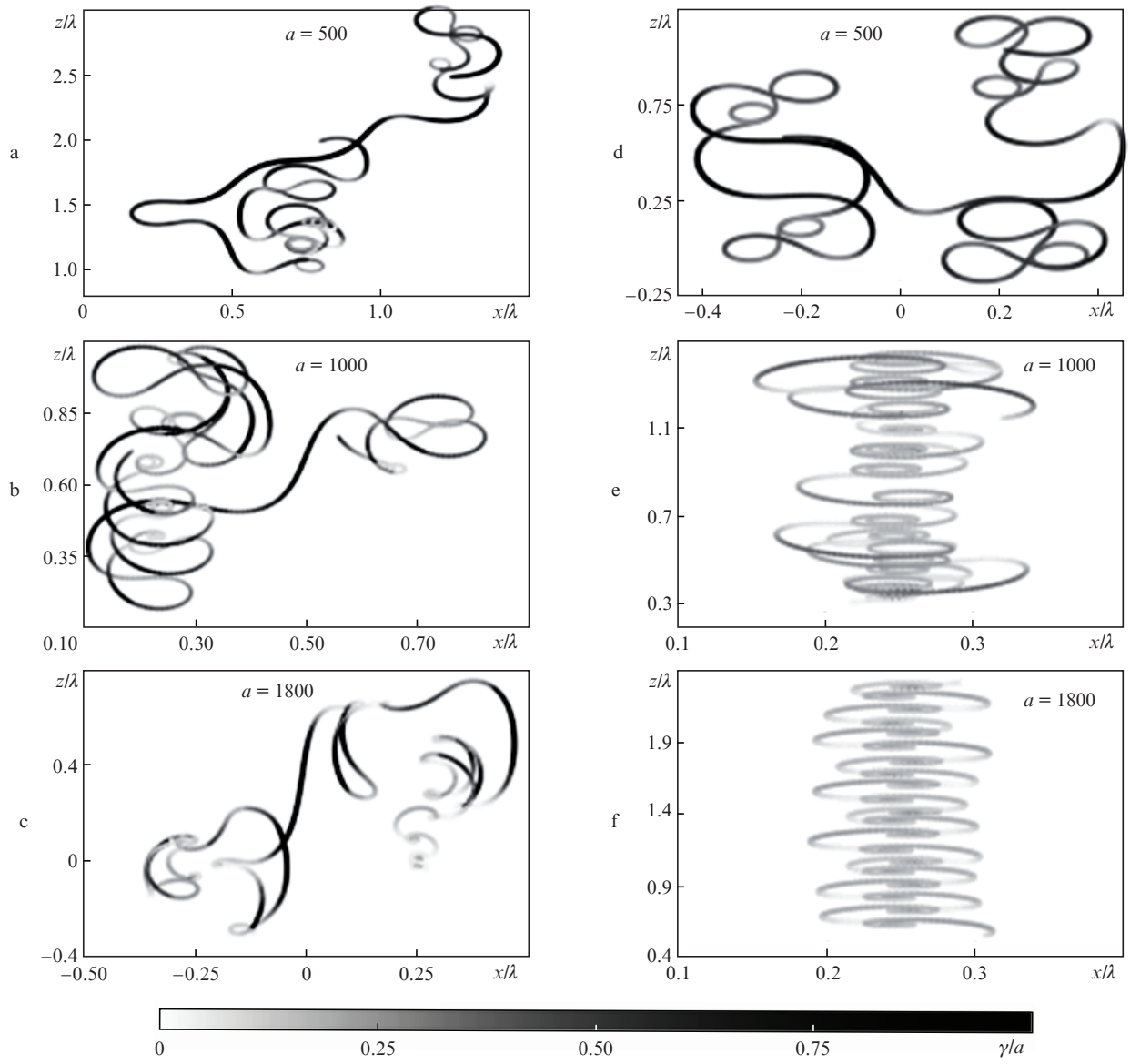

Figure 3. Electron trajectories in the regimes of relativistic stochasticity and NRT in the field of a plane standing linearly polarised wave at various amplitudes, obtained (a–c) within the framework of a quasi-classical approach to the description of radiation losses and (d–f) within the description of these losses with the use of the Landau–Lifshitz force with quantum corrections; γ is the gamma-factor of the electron.

force, substantially raise this threshold up to $a \approx 600$. Moreover, even despite the radiation stochasticity in a circularly polarised field, a 'pure' NRT regime is realised, whereas, in the case of linear polarisation, the particle are capable of leaving the capture region and then enter the region of another field node (compare Figs 3b and 3e). This is also clearly seen from Fig. 2a: as the amplitude increases, a narrower particle density distribution is formed near the node, but $n_{st}(x)$ does not vanish anywhere in this case.

We should note that the NRT regime due to these transitions is similar to the regime of relativistic stochasticity: the maximum density in both regimes is formed at the field node, and random particle transitions between the field nodes are observed (compare Figs 3a and 3b). However, in contrast to the regime of relativistic stochasticity, the ratio of maximum and minimum densities in the NRT regime is $\mu \gg 1$. At the threshold amplitude $a \approx 600$, the ratio is $\mu \approx 5$, and for $a = 1600$ we have $\mu \approx 86$. It is also worth noting that the NRT regime exists for all amplitudes, $a > 600$, but the regime's basin is greatly reduced and the particles become more localised near the field node with increasing amplitude (compare the distributions for $a = 1000$ and 10000 in Figs 2a and 2c). With increasing amplitude, in contrast to a decrease in spatial scale of particle oscillations in the framework of the force approach to the radiation loss description (compare Figs 3e and 3f), the particles in the quasi-classical approximation perform transitions from node to node of the field and also start to linger near the field antinode (Fig. 3c). In the integral distribution, this is manifested as an increase in the background density level between the node and antinode at $a > 1600$ (Fig. 2a). As a result, starting from $a \approx 2590$, when the rate of particle drift to the node becomes comparable with the rate of particle inflow into an antinode region, the ART regime arises.

At amplitudes $a > 2590$, the ART and NRT regimes can be realised simultaneously, a fraction of particles in each of them being determined by the initial conditions and the rate of particle transitions from regime to regime. The evidence of

particle motion in the NRT regime at these amplitudes is a maximum at the field node. In the ART regime, various structures are formed, differing in the set of extremes (local minima and maxima). The amplitude, starting from which a change in the set of extremes occurs, is considered as a threshold. The error in its determination $\Delta a \approx 50$ corresponds to the amplitude step, with which our numerical modelling was carried out near the threshold amplitudes. Based on the results of numerical simulations, three types of structures were revealed in the ART regime. At $2590 < a < 3000$, a maximum appears between the field node and its antinode, whereas a local minimum turns out located at the field antinode (Fig. 2b). For larger amplitudes $3000 < a < 4120$, a maximum instead of a minimum arises at the field antinode, so that two density maxima correspond to the ART regime (Figs 2b and 2c). At $a > 4120$, only maxima at the field node and antinode and a minimum between them remain (Fig. 2c). With increasing amplitude, the position of minimum is stabilised at point $x \approx 0.21\lambda$.

2.1. Particle motion in the ART regime

The variety of integral structures is explained by the special features of particle motion in the ART regime (Fig. 4). In this regime, particles oscillate both along the Poynting vector and the electric field during each half-period of the field near its antinode. As the amplitude increases, the particles on average approach the field antinodes, which is marked by vertical dashed lines for various field amplitudes in Figs 4a–4c. This fact has been earlier analysed both for a plane wave and for a tightly focused field in the form of a dipole wave [19]. In addition, at random time moments particles can pass through the field node and antinode. The fraction of particles that pass through the field antinode increases with increasing amplitude. It is most probable that a particle, after its transition, will fall into the neighbouring regions between the field node and antinode. The probability of the NRT regime is much less, because the NRT basin becomes much smaller compared to the ART basin. From a comparison of the trajectories in

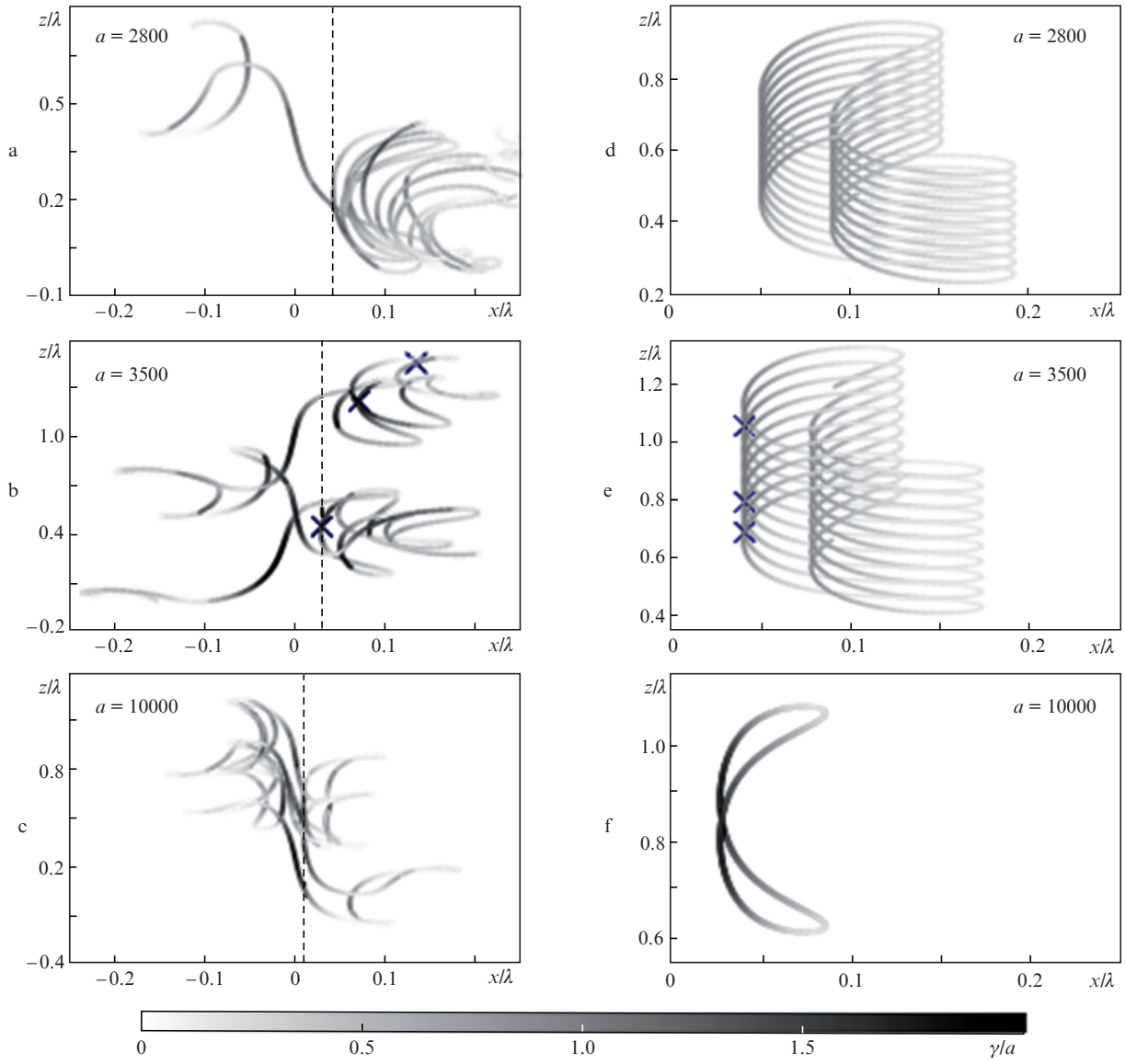

Figure 4. The same as in Fig. 3, but for the ART regime. Crosses in Fig. 3b and 3e indicate the position of particles at the same field phase. Vertical dashed lines correspond to the maximum approximation of particles to the field antinode without taking into account the transition through it.

Figs 4a–4c and 4d–4f it is clear that the transitions are caused by radiation stochastisity, since, in the description of losses by means of force, certain attractors are formed, which do not allow particle transitions. These attractors are characterised by a drift of particles along the electric field, but at large amplitudes ($a > 7500$) this drift is suppressed, and an eight-like trajectory is localised in space. Taking into account the radiation stochasticity, particles diffuse both along the Poynting vector and the electric field. Stochasticity does not allow perfect synchronisation of particles (compare Figs 4b and 4e), so the electron density in the region between the field node and antinode can be considered distributed along the Poynting vector within a segment of length l_{st} located at distance d_{st} from the field antinode:

$$f(x) = \tanh[\kappa(x - d_{st} + 0.5l_{st})] - \tanh[\kappa(x - d_{st} - 0.5l_{st})], \quad (4)$$

where κ is the coefficient characterising the growth rate of the function $f(x)$ at the edges of the specified segment. The function beyond this segment corresponds to particles migrating to the neighbouring regions. To calculate the model integral structures, we take into account the electron density distributions oscillating on both sides of a given field antinode. We neglect the contribution of particles coming from more distant regions and roughly assume that the oscillations (with the amplitude Δl) of the mass centre of electrons along the Poynting vector are described by the function $\Delta l|\cos\omega t|$. This function takes into account the change rate of the particle motion direction along the x axis in the vicinity of the field antinode at the time moment $t \approx 0.25Tj$ (j is an integer), when the electric field is close to zero. With given assumptions, the time dependence of the electron density distribution near the field antinode has the form

$$f(x,t) = f_R(x,t) + f_L(x,t), \quad (5)$$

where

$$\begin{aligned} f_R(x,t) = {} & \tanh[\kappa(x - d_{st} + 0.5l_{st} + \Delta l|\cos\omega t|)] \\ & - \tanh[\kappa(x - d_{st} - 0.5l_{st} + \Delta l|\cos\omega t|)], \\ f_L(x,t) = {} & \tanh[\kappa(x + d_{st} + 0.5l_{st} - \Delta l|\cos\omega t|)] \\ & - \tanh[\kappa(x + d_{st} - 0.5l_{st} - \Delta l|\cos\omega t|)]. \end{aligned} \quad (6)$$

The integral distribution is determined as follows:

$$n_{st}(x) = (0.5TM)^{-1}\int_0^{0.5T} f(x,t)\,\mathrm{d}t. \quad (7)$$

According to the properties of particle dynamics in the ART regime, as the amplitude increases, the values of l_{st}, d_{st}, and Δl decrease, while the coefficient κ increases. It is possible to select such values of these parameters that distributions (7) characterised by them would correspond to all possible integral structures in the field antinode vicinity in the ART regime (Fig. 2). The model structures with selected parameters are shown in Fig. 5.

The above qualitative model description of the particle ensemble dynamics also allows us to understand what causes a change in integral structures in the ART regime. With this aim in view, we introduce the parameter η, which determines a fraction of particles passing over the field antinode:

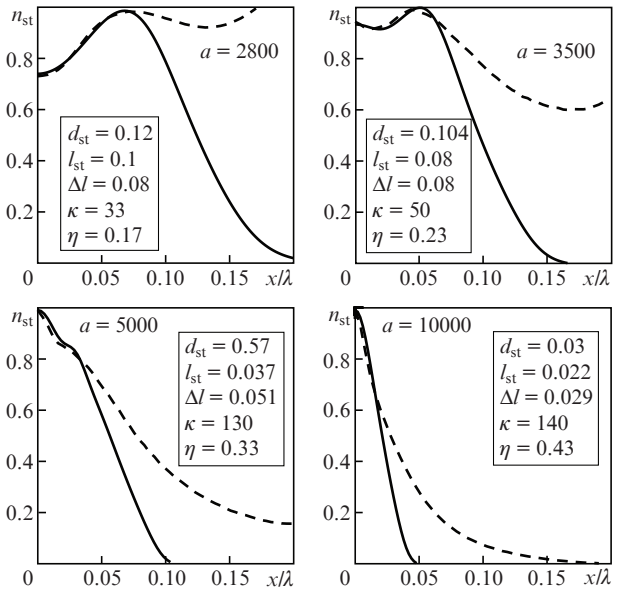

Figure 5. Model integral structures (solid curves) calculated by formula (7), and integral structures (dashed curves) obtained in numerical simulation (see Fig. 2). Figures show the amplitudes of plane standing linearly polarised waves corresponding to integral structures, and the parameters at which similar model distributions are observed.

$$\eta = \frac{\int_{-\infty}^{0} f_R(x,0)\,\mathrm{d}x}{\int_{-\infty}^{+\infty} f_R(x,0)\,\mathrm{d}x}. \quad (8)$$

To find this parameter, it is suffice to use only one of the functions f_R or f_L, which are localised mainly on the right or on the left of the field antinode, respectively. The chosen time moment $t = 0$ corresponds to the closest position of particles (on the ensemble average) with respect to the field antinode in accordance with expressions (6). The values of η for various field amplitudes are shown in Fig. 5. For amplitudes that correspond to the ART regime emergence, only a small fraction of particles can pass through the field antinode. The integral structure is characterised by a local density maximum in the intermediate region and a local density minimum at the field antinode. However, as the field amplitude increases, the parameter η also increases, and the local maximum appears directly at the electric field antinode, while the maximum in the intermediate region gradually decreases relative to the maximum at the field antinode and eventually disappears. An increase in the fraction of particles passing through the field antinodes with increasing amplitude is confirmed by the examples of trajectories in Fig. 4, obtained during the same period of time. Thus, it can be concluded that the rate of particle transitions through the field antinode determines all the structures observed in the ART regime.

3. Plasma structures taking into account the cascade development

In the previous section, we have considered the electron density structures formed by the interaction of particles with a plane linearly polarised wave. Such structures are determined by the particle motion. However, due to quantum processes, these structures can be modified in extremely strong fields. As

a result of particle motion in relativistically strong fields, a large number of gamma photons are emitted, which can decay into electron–positron pairs in a strong laser field, thereby generating an avalanche-like process, i.e. a QED cascade [1]. The particles are produced unevenly in space and time [22], so the cascade can substantially modify the electron density distribution and cause the appearance of extrema in the integral structure.

Integral structures can also be calculated with allowance for the QED cascade according to expressions (1). It is important to note that, due to an increase in the number of particles, the N_Σ value depends on time (in numerical simulation it depends on the time step number k). Numerical simulation has shown (Fig. 6) that integral structures become steady-state in a time less than $15T$, with their set being the same as without taking the cascade into account; however, there is an important difference. Threshold amplitude values at which the structures change are reduced. The error $\Delta a \approx 50$ in their determination is the same as without the cascade taken into account. Due to the presence of a cascade, the integral structures being characteristic of the ART regime appear at amplitudes $a > 1550$ (Fig. 6a), i.e. the threshold amplitude is 1.7 times smaller than in the case when the cascade is not taken into account. At these amplitudes (up to $a \approx 2590$), the NRT regime is realised without taking the cascade into account; however, the particles can be delayed for some time in an intermediate region between the field node and antinode. For the emergence of the ART regime without the cascade taken into account, it is necessary that the rate of particle inflow from the field node becomes equal to the rate of particle escape from the intermediate region to the field node. As the cascade develops, an additional source of particles appears in the intermediate region – the decay of photons into pairs, so the amplitude threshold of the ART regime decreases. Structures with maxima at the field node and between the field node and antinode are observed at the amplitudes $1550 < a < 2500$. The instantaneous distributions of electron densities with and without the cascade taken into account are shown in Fig. 7. The instantaneous structures are normalised to the maximum M of relevant integral structures. The cascade development leads to an increase in the fraction of particles located between the field node and antinode. In the case when the electric field (in relativistic units) exceeds by absolute value the magnetic field in the intermediate region (at t/T = 14.5, 14.55, 14.63, and 14.95 in Fig. 7), the density maximum appears in this region, whereas, if the cascade is not

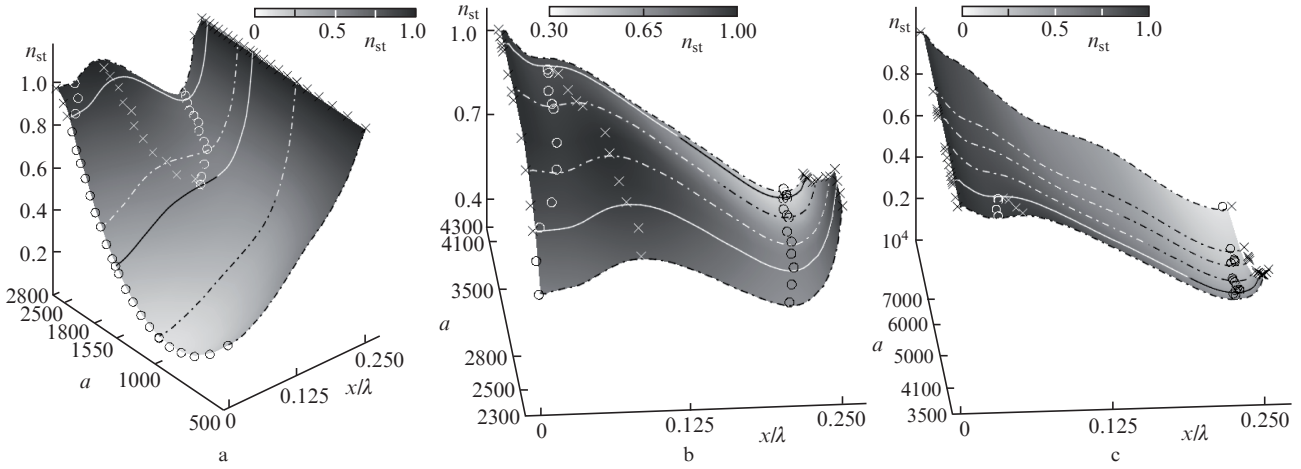

Figure 6. The same as in Fig. 2, but with allowance for the QED cascade.

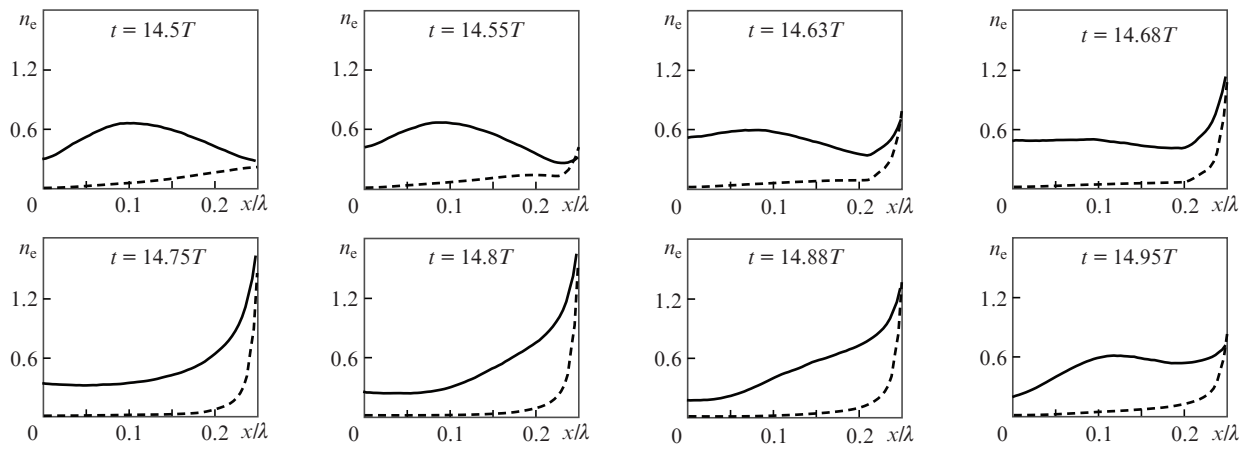

Figure 7. Instantaneous electron density distributions (solid curves) with and (dashed curves) without the cascade taken into account at the field amplitude $a = 1600$ of a plane standing linearly polarised wave.

taken into account, the cascade density increases virtually monotonically from the field antinode to node. In the case when electric field is smaller than magnetic field, the structures with and without taking the cascade into account are similar in shape, but the cascade increases the fraction of particles in the intermediate region.

In the range $2500 < a < 4100$ (Figs 6a and 6b), due to the special features of particle motion (as in the case without the cascade taken into account at $3000 < a < 4120$), a maximum in the field antinode appears. In this range, the ART regime is realised even without taking the cascade into account, so that produced particles are attracted to the field antinode. Due to stochasticity of particle production, the spatial scale of the distribution function becomes larger. This increases a fraction of particles passing through the field antinode and causes a maximum at the field antinode at lower field amplitudes compared to those determined without the cascade taken into account. We should note that the cascade development directly at the field antinode is suppressed, since the decay probability of photons emitted by particles as a result of their oscillations strictly along the electric field vector is negligible for the field amplitudes under consideration. In addition, in this range of amplitudes, the dynamics of produced particles with increasing amplitude leads to a shift of the integral structure maximum in the intermediate region towards to the field antinode.

With a further increase in the amplitude, the ART attractor moves closer to the field antinode, where the particles are rapidly attracted and spend a significant part of time during each half-period of the field. In this connection, even in spite of the inhomogeneity in time and space of the rate of particle production, the integral structure between the field node and its antinode vanishes at $a > 4100$ (Fig. 6b and 6c), though it can be observed in certain moments of time.

At the same time, the position of the minimum is not stabilised as in the case when the cascade is not taken into account, but shifts closer and closer to the field node, while the relative value of the integral structure maximum at the field node decreases. This occurs due to a reduction (an increase) of the basin of the NRT (ART) regime and a fraction of particles falling into this regime as a result of the cascade development. The dependence of spatial dimensions of the basins of these regimes on the field amplitude is reflected by integral structures without the cascade taken into account, as shown in Fig. 2c. The particle distribution corresponding to the NRT at large amplitudes is strongly localised near the field node. For this reason, a high spatial resolution is required to correctly describe the integral structures near the field node. For example, if the resolution is 256 points per wavelength, a maximum at the field node is changed to a minimum at $a \approx 10500$. However, an increase in the resolution to 512 points per wavelength allowed us to establish that the integral structure maximum is located at the field node. In the investigated range of amplitudes up to $a = 15000$ with an improved spatial resolution, the integral structure maximum at the field node is preserved. Thus, we can assume that, at $a > 10000$ and also at $4100 < a < 10000$, a maximum at the field node is preserved, the spatial scale of integral structure near the field node decreases, and the position of local minimum asymptotically tends to the field node. It should also be noted that, though the integral distribution becomes monotonically decreasing except for a small neighbourhood of the field node, the integral structure's spatial derivative is not monotonic, but has several maxima determined by the production of particles and their subsequent dynamics (Fig. 6c).

3.1. ART structure threshold with a cascade taken into account

In general, the integral structures in the ART regime with a cascade taken into account are quite complex, which is due not only to the complexity of particle motion determined in many respects by radiation losses and stochastic radiation, but also to the cascade dynamics being inhomogeneous in time and space. Above, various integral structures in the ART regime ($a > 1550$) have been qualitatively considered. However, the emergence of structures in the ART regime with allowance for the cascade can be investigated in more detail. To this end, it is necessary to analyse the dependence of the cascade growth rate and particle dynamics on the field amplitude.

As noted above, in the case of a linearly polarised wave, the cascade growth rate is not constant in time, in contrast to the case of circular polarisation [22]. However, the average growth of plasma density during the half-period of the field is exponential and can be characterised by the average rate Γ_{cs} of the cascade growth. After the integral structure has become steady-state, in order to find the Γ_{cs} value by means of numerical simulation, the maximum plasma density values n_e^{max} or the total number N_Σ of particles with a step equal to the half-period of the field are used. The cascade growth rate normalised to an inverse value of the field period is defined as

$$\Gamma_{cs} = \frac{2\ln[n_e^{max}(t + jT/2)/n_e^{max}(t)]}{j}$$

$$= \frac{2\ln[N_\Sigma(t + jT/2)/N_\Sigma(t)]}{j},$$

where j is an integer. The dependence of the cascade growth rate on the field amplitude is shown in Fig. 8a. On the one hand, in a plane wave, particles do not leave the interaction region, so there is no cascade threshold. In this regard, we can assume that the cascade should modify the plasma distribution at any amplitude. However, on the other hand, at low amplitudes ($a \ll 1000$), the cascade effect on plasma structures is insignificant, since the time interval $1/\Gamma_{cs}$ between the production of electron–positron pairs is much greater than the characteristic transition time to the regime of steady-state motion (relativistic chaos or NRT). In the regime of relativistic chaos, the transition time is approximately equal to the ratio of the field spatial inhomogeneity to the particle velocity along the field gradient, i.e. it constitutes $\sim 0.3T$, while the cascade growth rate is negligibly small. We should note that, in order to determine a small cascad growth rate for amplitudes $a < 800$, numerical simulation was carried out for a longer time interval of $300T$, since the transition time to the regime of the steady-state cascade development at small field amplitudes is much greater than the transition time to the steady-state motion.

At $a \approx 1000$, the cascade growth rate increases, and the electron structures with and without allowance for the cascade start to differ: in the first case, a fraction of particles between the field node and its antinode increases (see Figs 2a

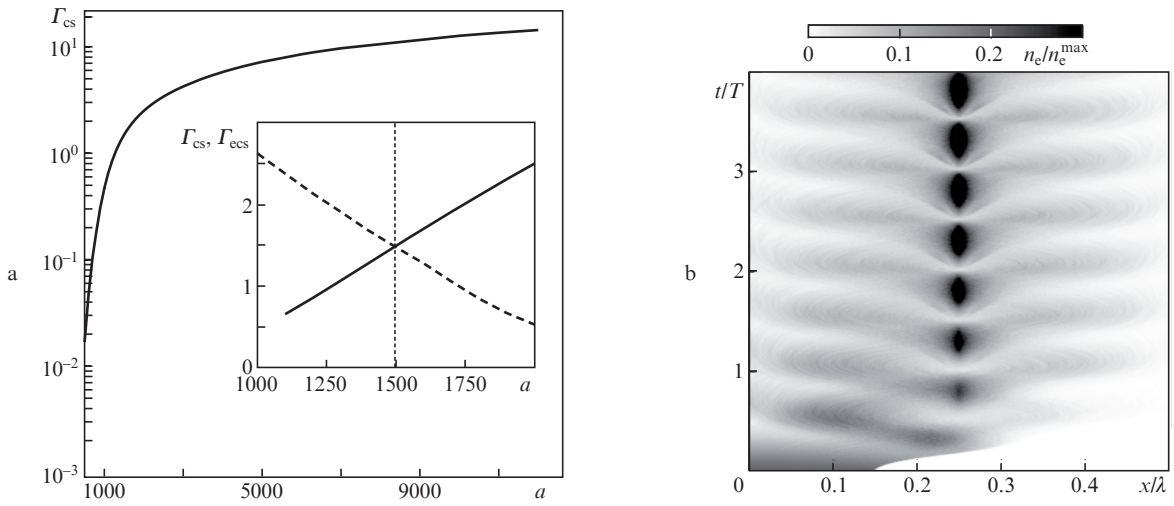

Figure 8. (a) QED cascade growth rate as a function of the field amplitude of a plane standing linearly polarised wave, and (b) spatiotemporal dynamics of electron motion in the field of this wave with the amplitude $a = 1600$ without allowance for the cascade. The inset shows the cascade growth rate (solid line) and the particle escape rate from the region $0 < x/\lambda < 0.15$ (dashed line) on a linear scale along the ordinate axis. The vertical dashed line defines a threshold of the ARP regime with allowance for the cascade.

and 6a). The particles falling into the intermediate region also require a time of about $0.3T$ to reach the regime of steady-state motion. As the field amplitude increases, the role of radiation losses increases, and the time to reach the NRT regime also increases, since, when a particle travels towards the field node, the 'recoil' due to emitted photons is directed in the opposite direction. At the same time, the cascade growth rate also increases. As a result, there is a balance between the rate of production of new particles and the rate of their transition to the steady-state motion, which determines the amplitude threshold for the appearance of structures characteristic of the ART regime. From a comparison of Figs 2a and 6a it is clear that this balance is observed when the particles move in the NRT regime. The particle trajectories and the distribution function dynamics in the NRT regime without taking the cascade into account are shown in Figs 3b, 3c and in Fig. 7.

Particles in this regime are concentrated mainly within the regions $0.15 + 0.5j < x/\lambda < 0.35 + 0.5j$. As shown above, in the steady-state regime the particle density due to the radiation stochasticity is nonzero outside these regions and is fixed at a certain level as a result of transitions through the field antinodes. To determine the rate of particle return to the field node, first we distributed particles uniformly within the segment $0 < x/\lambda < 0.15$ at the moment of time when the magnetic field equals zero. Second we found out how quickly the number of particles decreases within this segment. The segment corresponds to the region of the greatest difference in electron density distributions with and without taking the cascade into account at the time moment when magnetic field tends to zero ($t/T = 14.5$ in Fig. 7)

As a result of interaction with the field, particles oscillate along the Poynting vector, and each oscillation increases number of particles trapped into the NRT regime (Fig. 8b). Eventually, the initial perturbed distribution relaxes to the steady-state distribution with a corresponding equilibrium ratio of the number of particles located inside and outside the segment $0 < x/\lambda < 0.15$. In numerical simulation, we may approximately assume that the rate of particle escape to the regime of steady-state motion (the rate of their escape towards the field node) is determined as $\Gamma_{esc} = T/\tau_{esc}$, where τ_{esc} is the time during which the difference between the initial and steady-state number of particles inside the segment under consideration, averaged over the half-period, is reduced by a factor e. The dependence of Γ_{esc} on the field amplitude, determined from numerical simulation, is presented in Fig. 8a. The rates of distribution stabilisation and cascade growth are compared at $a \approx 1500$, which is very close to the threshold amplitude $a \approx 1550$ found from integral structures (Fig. 6a). Thus, numerical simulation confirms that the ART threshold with allowance for the cascade is determined by the balance of the particle escape rate to the field node and the cascade growth rate.

4. Conclusions

Thus, using numerical simulation, we have revealed and analysed electron–positron plasma structures in the field of a standing linearly polarised wave in a linear regime. Due to the inhomogeneous spatiotemporal dynamics of the distribution function, it is proposed to use the spatial distributions averaged over the half-period of the field (integral structures) to determine various regimes of particle motion. In the steady-state regime, these structures are stationary, and, in accordance with a set of their extrema, various regimes have been revealed and the amplitude thresholds for the emergence of these regimes have been found. In contrast to a circularly polarised field, the linearly polarised structures are more diverse, and, depending on the field amplitude, the integral structure maxima are observed not only at the field node, at the field antinode, or at the field node and antinode simultaneously, but also in the intermediate region between the field node and its antinode. These differences are dictated by a more diverse particle dynamics with allowance for radiation losses and a more complicated spatiotemporal cascade dynamics.

In the region of amplitudes $a < 1550$, a maximum at the field node and a minimum at the field antinode are observed. However, due to cascade development at $a > 1000$, a fraction of particles in the intermediate region increases, which ulti-

mately leads to a change in the integral structure at $a \approx 1550$. An additional maximum observed at $1550 < a < 2590$ appears in the intermediate region, which is associated with the balance of particle escape to the field node in the NRT regime and the production of particles due to the decay of gamma photons. For larger amplitudes ($2590 < a < 4100$), this maximum is determined by the ART regime. The integral structure maximum at the field antinode at $a > 2500$ is stipulated by particle transitions through the antinode, which occurs as a result of stochasticity of photon emission. In the range of amplitudes under consideration, the cascade development is suppressed directly at the field antinode. Note that, in the case of circular polarisation, a maximum at the field antinode is caused precisely by the maximum rate of the cascade growth in this region and appears at $a > 1100$ [27]. In terms of intensity, this threshold approximately corresponds to the threshold for appearance of a maximum in the intermediate region in the field of a linearly polarised wave.

At $a > 4100$, due to approach of the centre of mass of particles to the field antinode in the ART regime with increasing amplitude, and an increase in the fraction of particles passing through the antinode, the integral structure maximum in the intermediate region disappears, and only the maxima of integral structures at the field node and antinode remain. Unlike the case when the cascade is not taken into account, the positions of the structures' minima are not fixed at a distance of about 0.04λ from the field node, and, as the amplitude increases, they approach the field node where the integral structures' maxima over the entire region of amplitudes ($a \leqslant 10000$) are reached. High spatial resolutions near the field node are required to analyse the structures at even higher amplitudes with the use of numerical simulation, since the characteristic scale of the particle distribution corresponding to the ART regime decreases significantly with increasing amplitude. Numerical simulation at amplitudes up to $a = 15000$ with improved spatial resolution for the calculation of integral structures suggests that, at $a > 10000$, the positions of the structures' maxima at the field node are preserved, and the positions of their local minima tend asymptotically to the field node.

Note in conclusion that the rate of structure stabilisation under study strongly depends on the initial seed distribution of plasma density. This is especially true for amplitudes $1000 < a < 2000$ when the cascade growth rate is low, and also for short laser pulses. Moreover, the use of focused laser beams [23] may change the thresholds of the regimes detected for plane waves, since this enables the transverse escape of particles from the focal region and, as a consequence, a threshold of the self-sustained QED cascade arises. These factors may strongly affect the QED cascade structure in focused, linearly polarised laser beams, which requires further studies.

Acknowledgements. This work was supported by the Russian Foundation for Basic Research (Grant No. 17-52-45092) and the Presidium of the Russian Academy of Sciences (Extreme Light Fields and Their Interaction with Matter Programme, Agreement No. 007-03-2018-440). Numerical simulation was performed on high-performance MVS-100k and MVS-10p computers at the Joint Supercomputer Centre of the Russian Academy of Sciences.

References

1. Bell A.R., Kirk J.G. *Phys. Rev. Lett*., **101**, 200403 (2008).
2. ELI: www.eli-laser.eu.
3. VULCAN: www.clf.stfc.ac.uk/CLF/Facilities/Vulcan/.
4. XCELS: www.xcels.iapras.ru.
5. Nikishov A.I., Ritus V.I. *Zh. Eksp. Teor. Fiz*., **52**, 1707 (1967).
6. Gelfer E.G., Mironov A.A., Fedotov A.M., Bashmakov V.F., Nerush E.N., Kostyukov I.Yu., Narozhny N.B. *Phys. Rev. A*, **92**, 022113 (2015).
7. Gonoskov A., Bashinov A., Bastrakov S., Efimenko E., Ilderton A., Kim A., Marklund M., Meyerov I., Muraviev A., Sergeev A. *Phys. Rev. X*, **7**, 041003 (2017).
8. Gelfer E.G. *Quantum Electron*., **46**, 310 (2016) [*Kvantovaya Elektron*., **46**, 310 (2016)].
9. Tamburini M., Di Piazza A., Keitel C.H. *Sci. Rep*., **7**, 5694 (2017).
10. Artemenko I.I., Kostyukov I.Yu. *Phys. Rev. A*, **96**, 032106 (2017).
11. Jirka M., Klimo O., Vranic M., Weber S., Korn G. *Sci. Rep*., **7**, 15302 (2017).
12. Bulanov S.S., Esirkepov T.Z., Thomas A.G.R., Koga J.K., Bulanov S.V. *Phys. Rev. Lett*., **105**, 220407 (2010).
13. Fedotov A.M., Narozhny N.B., Mourou G., Korn G. *Phys. Rev. Lett*., **105**, 080402 (2010).
14. Nerush E.N., Kostyukov I.Yu., Fedotov A.M., Ruhl H. *Phys. Rev. Lett*., **106**, 035001 (2011).
15. Grismayer T., Vranic M., Martins J.L., Fonseca R.A., Silva L.O. *Phys. Plasmas*, **23**, 056706 (2016).
16. Vranic M., Grismayer T., Fonseca R.A., Silva L.O. *Plasma Phys. Controlled Fusion*, **59**, 014040 (2017).
17. Murav'ev A.A., Bastrakov S.I., Bashinov A.V., Gonoskov A.A., Efimenko E.S., Kim A.V., Meierov I.V., Sergeev A.M. *JETP Lett*., **102**, 148 (2015) [*Pis'ma Zh. Eksp. Teor. Fiz*., **102**, 173 (2015)].
18. Efimenko E.S., Bashinov A.V., Bastrakov S.I., Gonoskov A.A., Muraviev A.A., Meyerov I.B., et al. *Sci. Rep*., **8**, 2329 (2018).
19. Bashinov A.V., Efimenko E.S., Gonoskov A.A., Korzhimanov A.V., Muraviev A.A., Kim A.V., Sergeev A.M. *J. Opt*., **19**, 114012 (2017).
20. Kirk J.G., Bell A.R., Arka I. *Plasma Phys. Controlled Fusion*, **51**, 085008 (2009).
21. Duclous R., Kirk J.G., Bell A.R. *Plasma Phys. Controlled Fusion*, **53**, 015009 (2011).
22. Bashmakov V.F., Nerush E.N., Kostyukov I.Yu., Fedotov A.M., Narozhny N.B. *Phys. Plasmas*, **21**, 013105 (2014).
23. Jirka M., Klimo O., Bulanov S.V., Esirkepov T.Zh., Gelfer E., Bulanov S.S., Weber S., Korn G. *Phys. Rev. E*, **93**, 023207 (2016).
24. Baumann C., Pukhov A. *Phys. Rev. E*, **94**, 063204 (2016).
25. Kostyukov I.Yu., Nerush E.N. *Phys. Plasmas*, **23**, 093119 (2016).
26. Grismayer T., Vranic M., Martins J.L., Fonseca R., Silva L.O. *Phys. Rev. E*, **95**, 023210 (2017).
27. Bashinov A.V., Kumar P., Kim A.V. *Phys. Rev. A*, **95**, 042127 (2017).
28. Lehmann G., Spatschek K.H. *Phys. Rev. E*, **85**, 056412 (2012).
29. Gonoskov A., Bashinov A., Gonoskov I., Harvey C., Ilderton A., Kim A., Marklund M., Mourou G., Sergeev A. *Phys. Rev. Lett*., **113**, 014801 (2014).
30. Esirkepov T.Zh., Bulanov S.S., Koga J.K., Kando M., Kondo K., Rosanov N.N., Korn G., Bulanov S.V. *Phys. Lett. A*, **379**, 2044 (2015).
31. Bashinov A.V., Kim A.V., Sergeev A.M. *Phys. Rev. E*, **92**, 043105 (2015).
32. Bulanov S.V., Esirkepov T.Zh., Koga J.K., Bulanov S.S., Gong Z., Yan X.Q., Kando M. *J. Plasma Phys*., **83**, 905830202 (2017).
33. Bauer D., Mulser P., Steeb W.H. *Phys. Rev. Lett*., **75**, 4622 (1995).
34. Surmin I.A., Bastrakov S.I., Efimenko E.S., Gonoskov A.A., Korzhimanov A.V., Meyerov I.B. *Comput. Phys. Commun*., **202**, 204 (2016).
35. Gonoskov A., Bastrakov S., Efimenko E., Ilderton A., Marklund M., Meyerov I., Muraviev A., Sergeev A., Surmin I., Wallin E. *Phys. Rev. E*, **92**, 023305 (2015).
36. Baier V.N., Katkov V.M., Fadin V.S. *Izluchenie relyativistskikh elektronov* (Radiation of Relativistic Electrons) (Moscow: Atomizdat, 1973) p. 137.
37. Trubetskov D.I., Rozhnev A.G. *Lineinye kolebaniya i volny* (Linear Oscillations and Waves) (Moscow: Fizmatlit, 2001) p. 89.